doi:10.1017/S1431927621005468
Microsc. Microanal. 27 (Suppl 1), 2021


# Mapping metal/insulator nanodomains switching in $V_2O_3$ by variable-temperature electron spectromicroscopy investigations

Ibrahim Koita[1], Xiaoyan Li[2], Luiz H. G. Tizei[3], Jean-Denis Blazit[1], Nathalie Brun[1], Etienne Janod[4], Julien Tranchant[4], Benoît Corraze[4], Laurent Cario[4], Marcel Tencé[5], Odile Stéphan[1] and Laura Bocher[1]

[1]Université Paris-Saclay, CNRS, Laboratoire de Physique des Solides, 91405, Orsay, France, United States, [2]Université Paris-Saclay, CNRS, Laboratoire de Physique des Solides, 91405, Orsay, France, Ile-de-France, United States, [3]Université Paris-Saclay, CNRS, Laboratoire de Physique des Solides, 91405, Orsay, France, France, [4]Institut des Matériaux Jean Rouxel (IMN), Université de Nantes, CNRS, 2 Rue de la Houssinière, 44322 Nantes, France, United States, [5]Université Paris-Saclay, CNRS, Laboratoire de Physique des Solides, 91405, Orsay, France, ORSAY, France

Taming abrupt phase transitions existing in transition metal oxides is considered as a promizing approach for the development of advanced information processing and storage systems. $V_2O_3$ is a prototypical system exhibiting metal-to-insulator transitions (MITs) that can be activated under controlled external stimuli such as temperature (T), pressure, or chemical doping [1,2,3]. A precise and detailed understanding of these electronic transitions in Mott insulators and strongly correlated systems such as $(V_{1-x}Cr_x)_2O_3$ is essential to further enhance their potential capabilities for non-volatile memories [4] and neuromorphic applications [5].

The $(V_{1-x}Cr_x)_2O_3$'s phase diagram, established by the McWhan's pioneer studies [1] based on X-ray diffraction and transport measurements (Fig. 1a), contains two insulating (AFI and PI) and one metallic (PM) phases. Two types of MITs, both first order transitions, have been evidenced among the different structural, magnetic and electronic states probed at the macroscopic scale. The PI ↔ PM "pure" Mott transition can be achieved either by a low-level Cr doping ($x \geq 1.2\%$) or by applying pressure and involves a substantial volume change ($\approx 1.2$ %) at the transition without crystallographic symmetry breaking. Conversely, the PM ↔ AFI transition at ca. 160 K in pure $V_2O_3$ presents a symmetry breaking from rhombohedral to monoclinic, associated with (i) a magnetic transition to an antiferromagnetic ordered state, (ii) a large volume change (+1.4%) and (iii) a MIT yielding a resistivity change of 7 orders of magnitude. This T-driven MIT has been extensively studied at the macroscopic scale [6] and remains still a perfect arena to probe *in situ* the $V_2O_3$ structural and electronic evolutions at the finest scale.

More recently, the T-induced MIT has been mapped *in situ* by scanning photoemission spectroscopy [7], X-ray linear dichroism associated to PEEM [8] and nano-IR [9] revealing the microscopic coexistence of insulator/metallic (I/M) domains, but with 25 nm spatial resolution at best. Beyond this, micro-RX experiments associated with nano-IR mapping have investigated the competitive mechanisms between both structural and electronic phases. A clear shift between the rhombohedral/monoclinic and metal/insulator temperature transitions could be underlined and the presence of metallic monoclinic domains could be further inferred [9]. All these results drawn a more complex scenario than McWhan suggested first at the macroscopic scale.

Understanding the $V_2O_3$ electronic phase separation and its local mechanisms governing the the I/M domains dynamics across the MITs remains of key interests. Advanced monochromated electron

spectromicroscopes emerged these last years as real game-changers for nanomaterials characterization. The possibility of probing spectroscopic signatures with an ultra-high EELS resolution, i.e. down to few meV, extends a larger range of relevant electronic excitations (from IR to soft X-ray) available at the sub-nm scale and below [10]. These last instrumental capabilities can be further associated with *in situ* (variable-T and electrical biasing) options [11] providing a unique tool capable to give a direct, simultaneous and local access to structural, optical and electronic information, hence opening an entirely new avenue for exploring phase transitions at the finest scale. Here it will enable us to correlate the formation, nucleation, and dissolution of I/M nanodomains in $V_2O_3$ under variable-T conditions by investigating the electronic and structural competitions taking place at boundaries as thin as an atomic column. Variable-T UHR-STEM/EELS experiments were performed on the NION CHROMATEM 200 MC equipped of a double-tilt HennyZ cryo-holder using MEMS to vary continuously the temperature conditions from 120 K (Fig. 1b).

First, low-T thermal cycling across the electronic transition were monitored for probing and mapping the PM and AFI spectroscopic signatures along the [11-20] zone axis (Fig. 1c). Initially, Abe et *al.* performed low-loss and core-loss EELS at specific temperatures evidencing (i) a sharp spectral feature at ca. 1 eV in the PM state attributed to an interband plasmon that vanishes in the AFI phase and (ii) an energy shift of ca. 500meV on the O-K edge between PM and AFI states associated with a decrease in intensity in AFI related to the lower V3*d* - O2*p* hybridization [12]. Here we investigated the EELS low-loss signatures upon cooling and warming enabling us to highlight the temperature range of both electronic phases (Fig. 2a) and a 15K hysteresis between the MIT and IMT. We further mapped the low-loss PM and AFI signatures at the sub-nm scale upon thermal cycling confirming the coexistence of I/M nanodomains limited here by a defined domain wall (Fig. 2b). K-means clustering analyses [13,14] were applied on the low-loss hyperspectral data confirming an electronic homogeneity of each PM/AFI domains (Fig. 2c and 2d). Remarkably, periodic inhomogeneities of the HAADF intensity contrast can be observed solely in the corresponding AFI domain. These peculiar HAADF features were already characterized as twinned monoclinic domains observed in the AFI phase by Van Landuyt et *al.* [15] and Ayroles et *al.* [16]. Nanodiffraction 4D STEM is currently under investigations to identify the local distribution of the monoclinic/rhombohedral phases upon thermal cycling. All these combined results will enable us to correlate precisely the structural and electronic domains formation mechanisms and clarify the formation dynamics of the I/M domain wall.

The authors acknowledge funding from the EDPIF, the National Agency for Research under the JCJC program IMPULSE No. ANR-19-CE42-0001 and the program of future investment TEMPOS-CHROMATEM with the Reference No. ANR-10-EQPX-50, and the European Union's Horizon 2020 research and innovation program under grant agreement No 823717 (ESTEEM3).

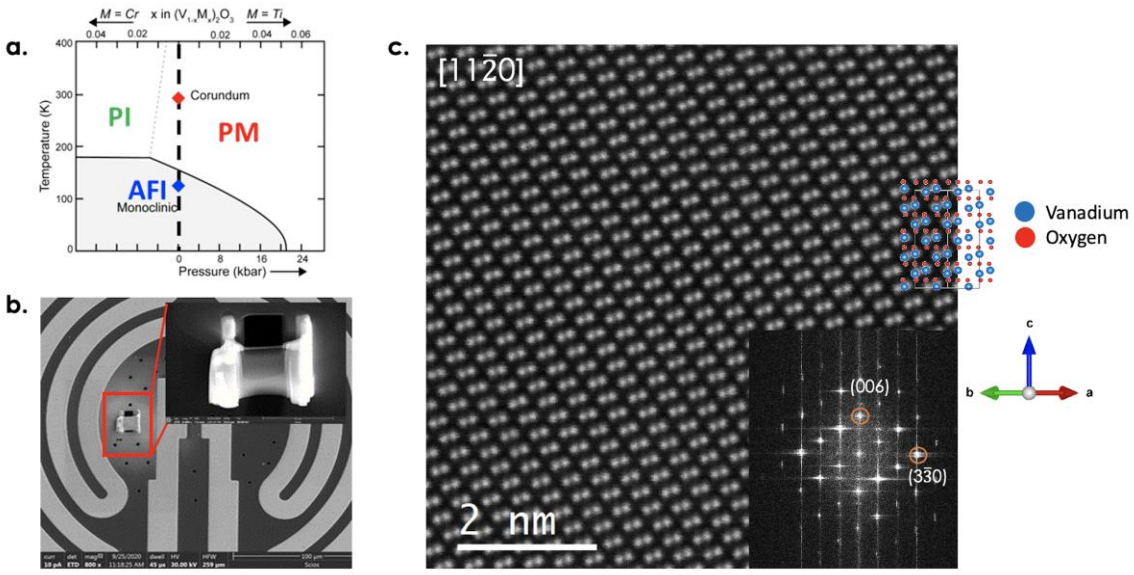


**Figure 1.** a. Phase diagram of $(V_{1-x}Mx)_2O_3$ (M for Cr or Ti) function of temperature, pressure and chemical doping adapted from McWhan et al. pioneer works [1,2,3]. b. SEM image of the heating/biasing MEMS used for the variable-T experiments with the enlarged view of the $V_2O_3$ thin lamella. c. STEM-HAADF image of $V_2O_3$ oriented in the [11-20] zone axis along with the structural model and the FFT in inset

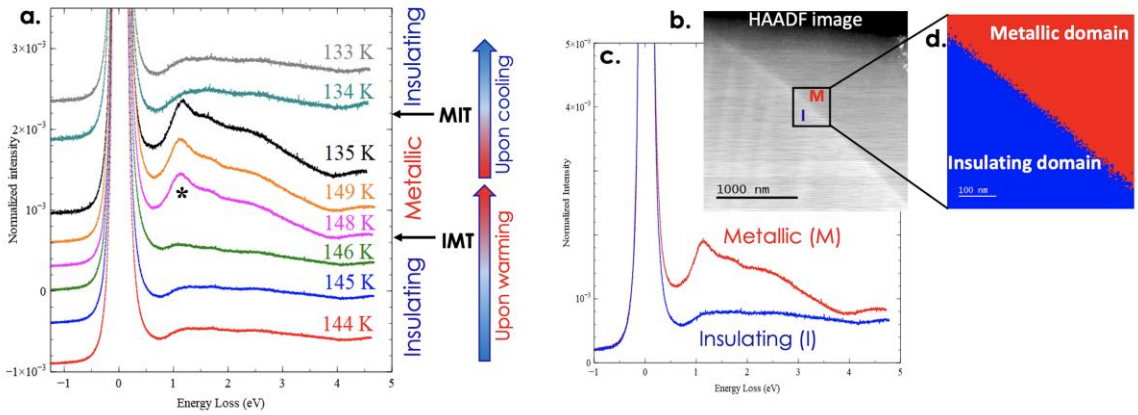


**Figure 2.** a. Low-loss EELS spectra (sum of 2000 spectra acquired in 100 ms each) probed every 1 K upon cooling and warming across the PM/AFI transition. The sharp feature at 1.1 eV marked with * is observed solely in the PM phase. For clarity, EELS spectra are shifted vertically with respect to each other. b. STEM-HAADF image acquired at 147 K, the related hyperspectral data were acquired in the region of interest (black square). c. Low-loss EELS spectra extracted from I/M domains in the region of interest. d. Map of the coexisting I/M domains acquired in the region of interest at 147 K and obtained by K-means clustering method

References

[1] D. B. McWhan, *et al.*, *Phys. Rev. Lett.* **1969**, *23*, 1384–1387.
[2] D. B. McWhan, *et al.*, *Phys. Rev. B* **1970**, *2*, 3734–3750.
[3] D. B. McWhan, *et al.*, *Phys. Rev. B* **1973**, *7*, 1920–1931.
[4] E. Janod, *et al*., *Adv. Funct. Mater.* **2015**, *25*, 6287–6305.
[5] P. Stoliar, *et al.*, *Adv. Funct. Mater.* **2017**, *27*, 1604740.
[6] A. Pergament, *et al*., *Phase Transit.* **2012**, *85*, 185–194.

https://doi.org/10.1017/S1431927621005468 Published online by Cambridge University Press

[7] S. Lupi, *et al*., *Nat. Commun.* **2010**, *1*, 105.
[8] A. Ronchi, *et al.*, *Phys. Rev. B* **2019**, *100*, 075111.
[9] A. S. McLeod, *et al.*, *Nat. Phys.* **2017**, *13*, 80–86.
[10] O. L. Krivanek, *et al.*, *Nature* **2014**, *514*, 209–212.
[11] B. H. Goodge, *et al.*, *Microsc. Microanal.* **2020**, *26*, 439–446.
[12] H. Abe, *et al.*, *Jpn. J. Appl. Phys.* **1998**, *37*, 584.
[13] P. Torruella, *et al.*, *Ultramicroscopy* **2018**, *185*, 42–48.
[14] A. Teurtrie. Phd thesis, *Université Paris Saclay (COmUE)* **2019**. https://tel.archives-ouvertes.fr/tel-02895558
[15] J. Van Landuyt, *et al*., *Mater. Res. Bull.* **1972**, *7*, 845–856.
[16] R. Ayroles, *et al.*, *J. Phys. Colloques* **1976**, *37*, C4-101 - C4-104.

https://doi.org/10.1017/S1431927621005468 Published online by Cambridge University Press